PCCP

Quantum scattering and quasi-classical trajectory calculations for the $H_2 + OH \rightleftharpoons H_2O + H$ reaction on a new potential surface

Sergei K. Pogrebnya,[a] Juliana Palma,[a] David C. Clary[a] and Julian Echave[b]

[a] *Department of Chemistry, 20 Gordon Street, University College London, London, UK WC1H 0AJ. E-mail: d.c.clary@ucl.ac.uk*
[b] *Centro de Estudios e Investigaciones, Universidad Nacional de Quilmes, Saenz Peña 180, 1876 Bernal, Argentina*

Received 7th October 1999, Accepted 1st December 1999

Six-dimensional (6D) quantum scattering calculations of reaction probabilities are reported for the $OH + H_2 \rightleftharpoons H_2O + H$ reaction. An arrangement channel hyperspherical coordinate method is used. A new potential energy surface due to Ochoa and Clary is employed. The results agree well with those calculated using the rotating bond approximation (RBA) and the quasi-classical trajectory (QCT) method. 6D quantum, RBA and QCT calculations of rate constants for the $OH + H_2$ reaction agree well with experiment. In addition, RBA calculations of differential cross sections for the $OH + D_2 \rightarrow HOD + D$ reaction and the photodetachment spectrum for H_3O^- also agree well with experiment. These results suggest that the new potential surface is reliable for this reason.

1. Introduction

The reaction

$$OH + H_2 \rightleftharpoons H_2O + H$$

has served as a benchmark for the development of quantum scattering theories capable of treating chemical reactions involving four atoms.[1] The first such calculations used the rotating bond approximation (RBA) in which the rotational motion of OH and vibrational motion of H_2 and H_2O were treated by explicit quantum mechanics while the rotational motion of H_2 and H_2O was treated with a reduced dimensionality approximation.[2] Various other approximations have also been applied to this reaction.[3,4] Accurate quantum scattering calculations have also been done more recently. This includes calculation of cumulative reaction probabilities[5] and wavepacket calculations of reaction probabilities selected in the initial ro-vibrational states.[6] In addition, coordinates specially tailored for this type of reaction, such as arrangement channel hyperspherical coordinates, have been applied to calculate the full state-to-state S matrix.[7] New time-dependent calculations have also been performed on this reaction.[8,9]

One reason why there have been so many calculations on this reaction is that it is the main route to H_2O in combustion[10] and is also important in interstellar chemistry.[11] Also, there have been a remarkable number of experiments on this reaction ranging from rate constants,[12] to differential cross sections,[13] to measurement of vibrational mode effects[14–16] and to photodetachment of H_3O^-.[17]

Almost all the quantum dynamics calculations mentioned above used a potential energy surface (PES) due to Schatz and Elgersma (SE), or minor modifications of it.[18] This potential is a fit to limited *ab initio* data and has the advantage that it is easy to use in both quantum scattering[2] and classical trajectory computations.[19] The more recent calculations have demonstrated some deficiencies of this potential, including a spurious well in the entrance channel, and a slightly incorrect geometry for the transition state.[2,20] In addition, this potential does not give accurate vibrational energy levels of H_2O and does not describe the full symmetry of the H_3O system.

A new PES recently developed by Ochoa and Clary[21] (OC) is free from the defects mentioned above and is based on more extensive *ab initio* calculations than the SE PES. It is, therefore, important to perform scattering calculations on this potential to test its accuracy. In addition, such computations serve as a test of the reliability of approximate methods when results are compared with those obtained by 6D quantum scattering calculations.

The aim of this paper is to report scattering calculations on the $OH + H_2$ reaction obtained with the new OC potential. The reaction probabilities, obtained with the 6D arrangement channel hyperspherical coordinate method,[7] are used to test the accuracy of the RBA and the quasi-classical trajectory (QCT) method for this system. A J-shifting approximation[22] allows the reaction probabilities to be turned into rate constants, and these are compared with experiment.[12] In addition, RBA calculations of differential cross sections for the $OH + D_2 \rightarrow HOD + D$ reaction are compared with experimental measurements[13] and a RBA computation of the spectrum for the photodetachment of H_3O^-, a process that needs the $OH + H_2 \rightleftharpoons H_2O + H$ potential surface for its description, is also compared with experiment.[17] The results described here thus represent a comprehensive test of the OC potential and a test of the accuracy of approximate dynamical methods for this important reaction.

Section 2 describes briefly the theoretical methods used in our calculations. Section 3 compares 6D quantum reaction probabilities with those obtained by the RBA and QCT. In Section 4, results of rate constants, differential cross sections and photodetachment spectra are compared with experiment to test the new potential energy surface. Conclusions are in Section 5.

2. Theory and numerical details

A. Potential energy surface

So far all modern dynamical calculations on the title reaction have been made on the potential energy surface developed by Schatz and Elgersma.[18] This PES is a many-body expansion

This journal is © The Owner Societies 2000

with a very simple formulation. However, it does have some flaws, including a spurious well in the entrance $H_2 + OH$ channel, which was corrected later.[2] It does not describe well the potential and vibrational energy levels of H_2O. Also, this PES does not describe the full symmetry of the H_3O system. The new OC PES[21] does not have these defects and is constructed with the aid of more recent *ab initio* calculations.[20] These *ab initio* data were fitted to an analytical form using the LAGROBO (largest angle generalisation of rotating bond order) model (see ref. 21 and references therein) in which the potential function is expressed as a many-process expansion of rotating bond order potentials. The LAGROBO model can guarantee that the PES does not have spurious structures and that it is continuous and smooth in the whole domain of configurations, even in zones for which no *ab initio* information is available. All properties of the OC PES were discussed in detail elsewhere.[21] For example, the characteristics of the transition state (geometry, energy, and frequencies) were found to be in good agreement with *ab initio* data. Another example illustrating an asymptotic property of the OC PES is given in Table 1. Here we compare the vibrational energies for H_2O calculated by using the OC PES with experimental data[23] and those calculated with the SE potential surface.[9] Note that the eigenvalues obtained on the OC PES derive from our 6D calculations in the asymptotic limit where the H atom is far away from the H_2O molecule. Clearly, the agreement with the experimental data is much better when the OC potential is used.

B. Full dimensional quantum scattering calculations

We use the arrangement channel hyperspherical coordinate method to carry out the full dimensional (6D) calculations for the $H_2 + OH \rightleftharpoons H_2O + H$ reaction.[7] In general, the theory used here is an extension to four-atom reactions of methods applied by Schatz,[24] Kuppermann and co-workers,[25] and Parker and Pack[26] to three-atom reactions. All relevant details of this method have been published in our previous paper.[7] Therefore only a brief outline is given here.

We consider reactions of the type $AB + CD \rightleftharpoons \{A + BCD, B + ACD\}$ where the bond CD is not broken during the reaction. The reaction channels are denoted $\alpha(A + BCD)$, $\beta(B + ACD)$, and $\gamma(AB + CD)$. Each channel, λ, is characterised by the set of six internal coordinates

$$R_\lambda, r_\lambda, z, \theta_\lambda, \vartheta_\lambda, \varphi_\lambda \tag{1}$$

and by the set of Euler angles denoted as Θ_λ. The coordinate z does not need a channel subscript because it corresponds to the CD bond which is common to all channels. Using hypercylindrical coordinates

$$z, \rho^2 = R_\lambda^2 + r_\lambda^2, \delta_\lambda = \arctan\left(\frac{r_\lambda}{R_\lambda}\right) \tag{2}$$

and the angles $\Gamma_\lambda = \{\theta_\lambda, \vartheta_\lambda, \varphi_\lambda\}$ we arrive at the Hamiltonian operator

$$H(\rho, z, \Theta_\lambda, \delta_\lambda, \Gamma_\lambda) = -\frac{\hbar^2}{2\mu}\frac{1}{\rho^5}\frac{\partial}{\partial\rho}\rho^5\frac{\partial}{\partial\rho} + H_S(z, \Theta_\lambda, \delta_\lambda, \Gamma_\lambda; \rho) \tag{3}$$

The explicit form of the surface Hamiltonian, H_s, is given in ref. 7.

For a given value of ρ, the channel surface states, $\Phi_n^{\lambda JM\varepsilon}$, are the simultaneous eigenfunctions of the channel surface Hamiltonian

$$H_S(z, \Theta_\lambda, \delta_\lambda, \Gamma_\lambda; \rho)\Phi_n^{\lambda JM\varepsilon} = E_n^\lambda(\rho)\Phi_n^{\lambda JM\varepsilon} \tag{4}$$

as well the total angular momentum, $\boldsymbol{J}$, and the parity operator of the whole four-atom system. The indices M and ε are the projection of $\boldsymbol{J}$ on the space fixed OZ axis and the coordinate inversion parity, respectively. We are looking for $\Phi_{n\lambda JM\varepsilon}$ as an expansion over the channels basis functions

$$B^{JM\varepsilon}_{\lambda v_\lambda w j_\lambda \Omega_\lambda} = Y^{JM\varepsilon}_{j_\lambda\Omega_\lambda}(\Theta_\lambda, \Gamma_\lambda)\chi_{v_\lambda}(\delta_\lambda)\chi_w(z) \tag{5}$$

The definitions of the BF angular momentum eigenfunctions, $Y^{JM\varepsilon}_{j_\lambda\Omega_\lambda}$ and the channel "vibrational" basis functions $\chi_v(\delta)$ and $\chi_w(z)$ are given in ref. 7. Note that j_λ is the collective index to denote $(j_1^\lambda, j_2^\lambda, j_{12}^\lambda)$. For the α and β channels, $\boldsymbol{j}_1^{\alpha(\beta)}$ is the orbital angular momentum operator of B and A with respect to the diatom CD, respectively. For the γ channel, $\boldsymbol{J}_1^\lambda$ is the rotational angular momentum operator of diatom AB. For all channels, $\boldsymbol{j}_2^\lambda$ denotes the rotational angular momentum operator of CD. Vectors $\boldsymbol{j}_1^\lambda$ and $\boldsymbol{j}_2^\lambda$ are coupled to form $\boldsymbol{j}_{12}^\lambda = \boldsymbol{j}_1^\lambda + \boldsymbol{j}_2^\lambda$ which, for the α and β channels, corresponds to the total angular momentum operator of the triatoms BCD and ACD, respectively.

Having obtained the channel surface eigenfunctions we use them to expand the total surface states as

$$\psi_k(z, \delta_\lambda, \Gamma_\lambda, \Theta_\lambda; \rho) = \sum_{\lambda', n} C_{nk}^{\lambda'}\Phi_n^\lambda(z, \delta_{\lambda'}, \Gamma_{\lambda'}, \Theta_{\lambda'}; \rho) \tag{6}$$

where, for simplicity, we drop all symbols except those that describe an arrangement channel and a state number. Note that functions Φ_n^λ and $\Phi_m^{\lambda'}$ with $\lambda \neq \lambda'$ are orthogonal only at large ρ. At small ρ they overlap to couple the different arrangement channels. The diagonalization of the surface Hamiltonian, H_s, in the basis (6) leads to the generalised eigenvalue problem as described in ref. 7.

Once the total surface functions have been calculated on a grid of fixed values of ρ, we use the R-matrix propagation method[27] to find the solution of the Schrödinger equation for the scattering wavefunction $\Psi_{\lambda_0 n_0}$

$$H\Psi_{\lambda_0 n_0} = E\Psi_{\lambda\lambda_0 n_0} \tag{7}$$

where the Hamiltonian H is given by eqn. (3), E is total energy, and λ_0 and n_0 label the initial channel and state, respectively. A significant advantage of this approach is that it is very easy to calculate reaction probabilities for more than one energy once a calculation has been done at the first energy, since the surface states are energy independent. The close-coupling expansion is used to solve eqn. (7), starting from a small value of ρ in the classically forbidden region and integrating out to large ρ, where appropriate boundary conditions are applied to obtain the final S matrix elements $\{S_{\lambda n, \lambda_0 n_0}\}$.

For a given total energy E, once the whole S matrix has been obtained, we can calculate different reaction probabilities, namely, the state-to-state probabilities

$$P_{\lambda n\leftarrow\lambda_0 n_0}(E) = |S_{\lambda n, \lambda_0 n_0}(E)|^2 \tag{8}$$

the initial state-selected ones

$$P_{\lambda\leftarrow\lambda_0 n}(E) = \sum_n P_{\lambda n\leftarrow\lambda_0 n}(E) \tag{9}$$

and the cumulative probability

$$P_{\lambda\leftarrow\lambda_0}(E) = \sum_{\text{sym}}\sum_n\sum_{n_0} P_{\lambda n\leftarrow\lambda_0 n}(E) \tag{10}$$

Here besides the initial states n_0, and final ones, n, we also sum over the four symmetry cases.

In our previous study[7] we have applied the above method to the $H_2 + OH \rightleftharpoons H_2O + H$ reaction where the length of the OH bond was fixed. Here we carry out the full (6D) dimensional calculations using the OC PES for $J = 0$.

We have carried out the calculations in four, "even(odd–even(odd)", symmetry cases. Here the first type of the symmetry is that associated with the coordinate inversion and the second one is the permutation symmetry of two H atoms. Due to the symmetry of the problem, only two sets of channel surface functions, namely, $\gamma(H_2 + OH)$ and $\alpha(H_2O + H)$, need

Table 1 Vibrational energies (in cm^{-1}) of H_2O with the ground rotational state

Vibrational state	OC PES	SE PES, ref. 9	Observed[23]
010	1594	1427	1595
020	3155	2645	3151
100	3645	3516	3657
001	3739	3702	3756
030	4684	3597	4667
110	5191	4895	5235
011	5293	5056	5331

[a] The zero energy is defined as the ground vibrational state.

to be calculated explicitly. Since the numerical details of the calculations within every block are similar we restrict the description to the "even–even" case.

For the γ channel, the basis set is constructed as follows. We use $N_{v_\gamma} = 2$ sector "vibrational" functions $\chi_{v_\gamma}(\delta_\gamma)$ and $N_w = 3$ functions $\chi_w(z)$. Each vibrational function $\chi_n(x)$ is associated with a number of rotational functions with j up to the maximum value $j_n^{\max}$. We have used $(j_1^\gamma)_0^{\max} = 12$, $(j_1^\gamma)_1^{\max} = 6$ for H_2, $(j_2^\gamma)_0^{\max} = 12$, $(j_2^\gamma)_1^{\max} = 8$, $(j_2^\gamma)_2^{\max} = 4$ for OH, and all possible values of $|j_1^\gamma - j_2^\gamma| \leqslant j_{12}^\gamma \leqslant (j_1^\gamma + j_2^\gamma)$. Note that due to the symmetry, only even rotational functions of H_2 are included in the basis set. The rotational functions of H_2 and OH are coupled to produce the functions $Y^{J=0,\,M=0,\,\varepsilon}_{j_\gamma \Omega_\gamma = 0} = Y^\varepsilon_{j_\gamma}$ of eqn. (5) as described in ref. 7. Since we consider only $J = 0$, the inversion parity for all channels is given by

$$\varepsilon = (-1)^{j_1^\gamma + j_2^\gamma + j_{12}^\gamma} \tag{11}$$

The method of calculating vibrational basis functions, $\chi_{v_\gamma}(\delta_\gamma)$ and $\chi_w(z)$, is given in ref. 7. In total, we used $N_{\text{tot}}^\gamma = 1102$ ro-vibrational basis functions when calculating the surface wavefunctions in the γ channel.

For the α channel, the description of the basis set is similar to the above with some exceptions. We have used $N_{v_\alpha} = 3$ and $N_w = 3$ with $(j_1^\alpha)_0^{\max} = (j_2^\alpha)_0^{\max} = 20$, $(j_1^\alpha)_1^{\max} = (j_2^\alpha)_1^{\max} = 18$, and $(j_1^\alpha)_2^{\max} = (j_2^\alpha)_2^{\max} = 8$. However, in this case the use of all possible j_{12}^α will make the size of the basis set too big. Therefore, we reduce the size of the basis set by introducing $(j_{12}^\alpha)_{v_\alpha w}^{\max}$ for each pair of (v_α, w). These values are given in Table 2. Such a basis set consists of $N_{\text{rot}}^\alpha = 2696$ rotational functions and the total number of ro-vibrational functions is equal to $N_{\text{rot}}^\alpha = 9997$. To reduce further the size of the basis we used the procedure described previously.[7] Keeping in mind that at the asymptotic limit (j_{12}^α) is a good quantum number, we, at the first stage, diagonalize the surface Hamiltonian in each (j_{12}^α) block. Then from each this block we pick up the lowest $M_{j_{12}}^\alpha$ states and use these $M_\alpha = \sum_{j_{12}} M_{j_{12}}^\alpha$ states as a new basis set to make a final diagonalization of the surface Hamiltonian for the α channel. In the present calculations we use $M_\alpha = 3324$.

The closed-coupled equations were solved using the R matrix propagation method[27] with the integration limits of $\rho_a = 2.8\ a_0$ and $\rho_b = 12.0\ a_0$. The whole region was divided into 92 equally spaced sectors. At every sector $N_\alpha = 1300$ and $N_\gamma = 500$ α and γ states, respectively, were mixed to obtain the total surface functions.

C. RBA calculations

The computational and numerical details of applying the RBA to the $OH + H_2 \rightleftharpoons H_2O + H$ reaction are described in detail elsewhere.[2,28] The method implemented here gives state-to-state S matrix elements and reaction probabilities selected in the rotational states of OH, vibrational states of H_2 and the bending and local OH stretching vibrations of H_2O. These results for the local OH stretching vibration refer to a sum over probabilities into both the symmetric and asymmetric stretch vibration of H_2O. Cumulative reaction probabilities, for comparison with the accurate results, and rate constants, for comparison with experiment, can be obtained by application of a reduced dimensionality theory that requires the frequencies correlating with the H_2 rotational motion at the transition state.[22,28] Application of the coupled states approximation allows S matrix elements to be obtained for different values of the total angular momentum J so that integral and differential cross sections can be calculated.[20] The method can also be adapted to calculate the photodetachment spectrum for H_3O^-, a process for which $OH + H_2$ or $H_2O + H$ are the products, and full details are given elsewhere.[29]

Table 2 Values of $(j_{12}^\alpha)_{v_\alpha w}^{\max}$ used in the computations

(v,w)	0,0	1,0	2,0	0,1	1,1	2,1	0,2	1,2	2,2
$j_{12}^{\max}$	22	18	12	18	16	10	10	8	4

D. QCT calculations

We also used the QCT method to calculate cumulative and various initial state-selected reaction probabilities for $J = 0$ and thermal rate constants. Note that we calculate thermal rate constants using the standard QCT procedure and, therefore, do not derive them from QCT probabilities obtained at $J = 0$. The methodology of the QCT calculations which we carry out here, has been described previously.[30] Here we just review the main aspects referred to the choosing of the initial conditions for the trajectories, and give some numerical details.

For each initial state of OH and H_2, the internal energies and bond lengths were selected according to the prescriptions for a rotating Morse oscillator.[31] The initial orientation and the rotation plane of each diatomic were selected at random, following standard procedures.[32]

When calculating the probabilities for $J = 0$, the coordinates and momenta for the relative motion must be selected by such a way that they compensate the angular momentum due to the rotation of the reactants. To do so, we first obtain the Cartesian components of the rotational angular momentum of H_2 and OH, $\boldsymbol{j}_1$ and $\boldsymbol{j}_2$, respectively. This can be done once the initial bond lengths, orientations and planes of rotation are determined. Then, we calculate the orbital angular momentum, $\boldsymbol{j}_R$, which for zero total angular momentum is given by

$$\boldsymbol{j}_R = -(\boldsymbol{j}_1 + \boldsymbol{j}_2) \tag{12}$$

From $|\boldsymbol{j}_R|$ and the collisional energy E_C, we assign coordinates and momenta for the relative motion as

$$\begin{aligned} R_x &= -(R_0^2 - b^2)^{1/2}; \quad R_y = b, \quad R_z = 0 \\ P_{R_x} &= (2\mu E_C)^{1/2}; \quad P_{R_y} = 0, \quad P_{R_z} = 0 \end{aligned} \tag{13}$$

where $b = -|\boldsymbol{j}_R|/(2\mu\, E_c)^{1/2}$, R_0 is the initial distance between the centres of mass of the reactants and μ is the reduced mass for the relative motion. Finally, we rotate the vectors $\boldsymbol{R}$ and $\boldsymbol{P}_R$ by an angle χ around the y axis and then by an angle ϕ around the z axis so that eqn. (12) is fulfilled. These angles are given by

$$\chi = \arccos\left(\frac{j_{R_z}}{|\boldsymbol{j}_R|}\right)$$

$$\phi = \begin{cases} \arccos\left(\dfrac{j_{R_x}}{|\boldsymbol{j}_R| \sin\chi}\right) & \text{if } j_{R_y} > 0 \\ 2\pi - \arccos\left(\dfrac{j_{R_x}}{|\boldsymbol{j}_R| \sin\chi}\right) & \text{if } j_{R_y} < 0 \end{cases} \tag{14}$$

To calculate the cumulative probabilities for $J = 0$ we use a Monte Carlo procedure. It consists of selecting the initial states of the reactants at random, with uniform probability, from the set of the allowed energy levels at the given total

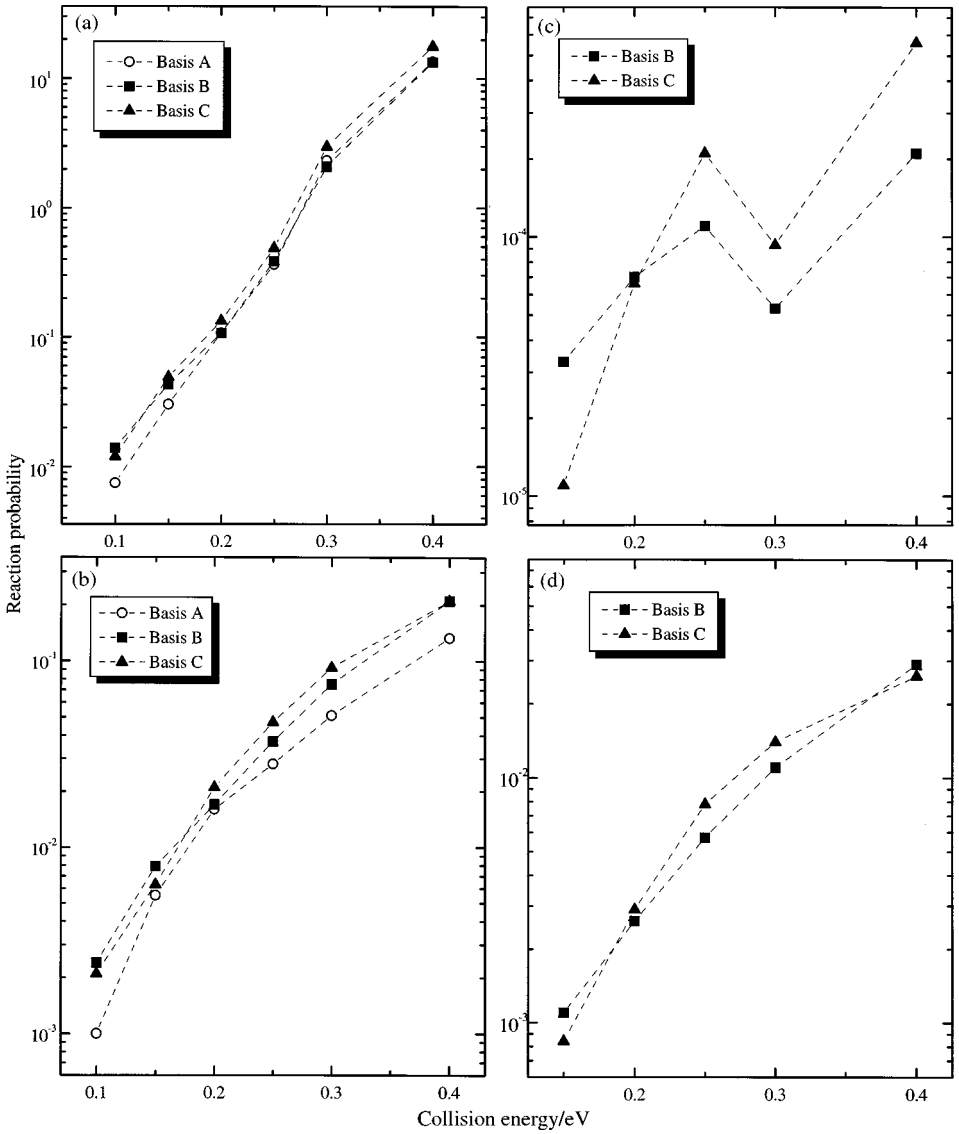

Fig. 1 (a) Cumulative probabilities for the $H_2 + OH \rightarrow H_2O + H$ reaction obtained with different basis sets (as described in Table 3) in the 6D quantum calculations. The collision energy is measured from the energy of $H_2(0,0) + OH(0,0)$. (b) Initially state-selected reaction probabilities for $H_2(0,0) + OH(0,0) \rightarrow H_2O + H$ summed over all product H_2O ro-vibrational states. (c) Convergence test for the state-to-state, $H_2(0,0) + OH(0,0) \rightarrow H_2O(0,0,0;2) + H$, reaction probabilities. (d) The same as part (c) but summed over H_2O rotational states, to give reaction probabilities for $H_2(0,0) + OH(0,0) \rightarrow H_2O(0,0,0) + H$.

energy. Then each trajectory is weighted by a degeneracy factor g, that for $J = 0$ is given by

$$g = 2 \min(j_1, j_2) + 1 \quad (15)$$

When calculating the rate constants, the initial state of the reactants, the collisional energy and the impact parameter are selected at random. To select the initial states of the reactants we used the Boltzmann distributions of the ro-vibrational levels for the corresponding rotating Morse oscillators. For the impact parameter we used a uniform distribution within the interval $[0, b_{max}]$. The value of b_{max} was determined from the analysis of the opacity functions for different initial states of the reagents. In this analysis we did not include vibrational excited states of the reactants as they are hardly occupied at the temperatures we considered ($T \leqslant 700$ K). The collisional energy was selected from the interval (E_{min}, ∞) using the standard formulas.[32] The value of E_{min} was chosen from the analysis of the threshold behaviour of the probabilities for $J = 0$.

In the calculation of reagent state-selected probabilities we used between 1500 and 3000 trajectories per initial state, per collisional energy. In the calculation of cumulative probabilities we used between 1500 and 2000 trajectories depending on the total energy. More trajectories were run at the lower energies to reduce the statistical uncertainty. In the calculation of thermal rate constants we used between 6000 and 10 000 trajectories per temperature. Again, more trajectories were used at the lower temperatures to improve the statistics. The maximum impact parameter was set at $b_{max} = 3.1\ a_0$, and the minimum collisional energy was set at $E_{min} = 0.08$ eV. Only

Table 3 Basis sets ("even–even" case) used in 6D quantum calculations

Basis set	N^{γ}_{tot}	N^{α}_{rot}	N^{α}_{tot}	M_{α}	N_{γ}	N_{α}
A	763	2400	7606	2526	400	1200
B	1102	2400	9039	3003	500	1300
C	1102	2696	9997	3324	500	1300

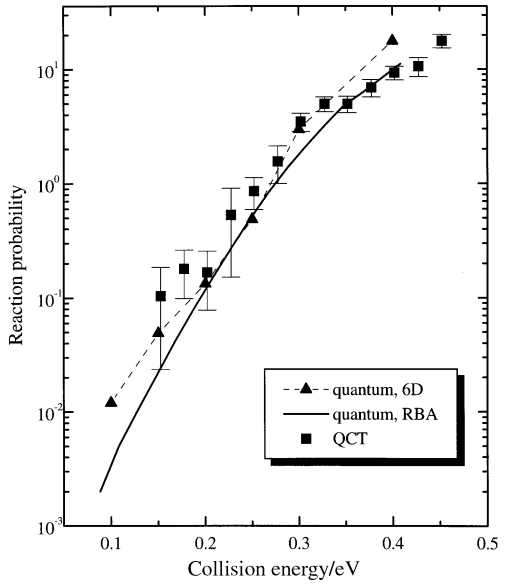

Fig. 2 Cumulative probabilities for the $H_2 + OH \rightarrow H_2O + H$ reaction calculated with the 6D quantum, RBA and QCT methods. The collision energy is measured from the energy of $H_2(0,0) + OH(0,0)$.

trajectories for which the conservation of total energy was better than 5×10^{-4} eV were considered in the calculations. In the calculation of probabilities for $J = 0$ we also ignored trajectories for which the total angular momentum at the end of integration was greater than $5 \times 10^{-4}\ \hbar$.

3. Reaction probabilities

In this section we present the results of $J = 0$ reaction probabilities for the $H_2 + OH \rightarrow H_2O + H$ obtained with three different methods. Using the results of 6D quantum scattering calculations as a benchmark, we test the accuracy of the QCT and RBA approximate methods for this reaction using the OC PES.

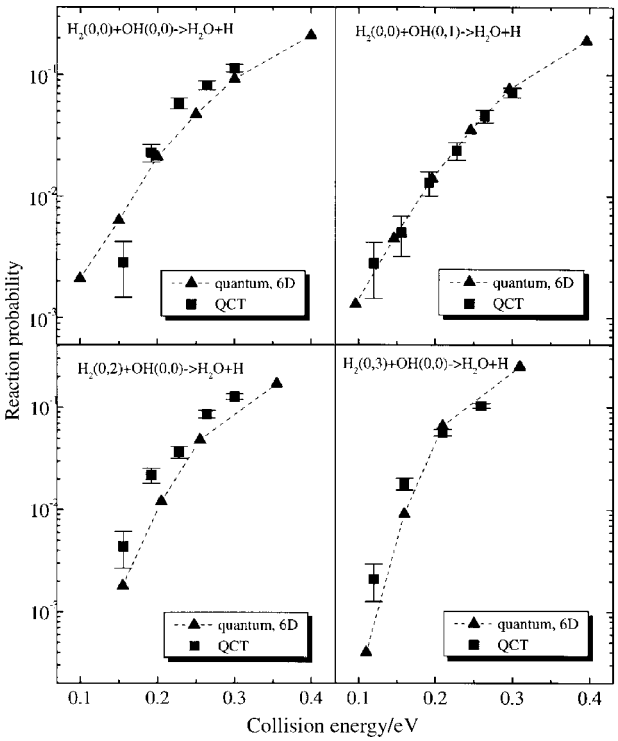

Fig. 3 Initial state-selected probabilities for the $H_2(0, j_1) + OH(0, j_2) \rightarrow H_2O + H$ reaction as a function of the collision energy measured from the energy of $H_2(0, j_1) + OH(0, j_2)$. The probabilities are summed over all product states of H_2O. 6D quantum and QCT results are compared.

One of the most important aspects of any quantum scattering calculations is a test of the convergence of the reaction probabilities with the increase of the ro-vibrational basis set used in the scattering computations. The other parameters, such as the size of the grid on which the channel surface wavefunctions are defined, the number of sectors, the value ρ_b at which the boundary conditions are applied, are also important. The results of such a test are illustrated in Figs. 1(a)–1(d), where we present the 6D quantum reaction probabilities calculated within different basis sets. The sizes of these basis sets are given in Table 3. As one may expect, the best convergence is achieved when describing the least detailed property such as the cumulative probability (Fig. 1(a)). As the collision energy increases, the difference between the results obtained with two largest basis sets (B and C) increases from about 10% to 25% with an average difference of 18%. This just reflects the fact that as the collision energy becomes higher the size of the basis set should be larger. Fig. 1(b) shows the initial state-selected probabilities to be converged within the similar level of accuracy. Clearly, it is extremely difficult to converge small individual state-to-state probabilities as it may be seen from Fig. 1(c). However, when they are partially summed (for example, over the final H_2O rotational states), these probabilities exhibit much better convergence (Fig. 1(d)). We conclude that the largest basis set used here is sufficient to estimate probabilities summed over product rotational states of H_2O within an accuracy of about 20%, but larger basis sets will be needed to converge the reaction probabilities selected in the individual rotational states of H_2O. One should remember that even with basis sets reported here, 6D quantum scattering calculations require a vast amount of computational resources. Nevertheless the calculations with a larger basis set are currently under way and will be reported in future work.

In Fig. 2 we present the cumulative probabilities calculated using different methods. For the collision energies above 0.15 eV the average difference between RBA and 6D results does not exceed 22%. However, at the lowest collision energies the RBA cumulative probabilities tend to fall several times below 6D ones. We believe this due to the approximate nature of RBA which does not treat all degrees of freedom. One sees that the QCT results follow the quantum curves well except for low collision energies. Near threshold, the QCT probabilities exhibit a non-monotonic behaviour and seem to be too large at the lowest collision energies. It is well known, that QCT fails at low energies to describe the dynamics of the reaction because of two reasons, the lack of zero point energy and the lack of tunnelling. The QCT probabilities may be above or below the quantum ones depending on which of these effects is more important. Our current results suggest that for the OC PES the lack of zero point energy is the dominant effect and, therefore, we find the QCT cumulative probabilities to be above the quantum ones. Also, when probabilities are very small, the QCT method has a problem due to its statistical nature. As the reaction probability decreases the relative error given by the QCT method increases. We believe that this statistical uncertainty is the reason for the non-monotonic behaviour observed near the threshold. The problem can be eliminated by running a greater number of trajectories at the lowest collision energies. However, this will make the calculations very costly.

We also note that the main contributions to the sum (10) are given by "even–even" and "odd–even" symmetry cases. The "even(odd)–odd" symmetry cases correspond to the out-of-plane rotations only. Since the transition state of the $OH + H_2 \rightarrow H_2O + H$ system is planar, they give a small contribution to the cumulative probability.

In Fig. 3 we compare various initial state-selected probabilities obtained using 6D quantum scattering calculations with the largest basis set (C) and QCT. We can see that the agreement is again good. As one may expect, the maximum deviation of the QCT results from the quantum ones tends to appear at small collision energies.

4. Comparison with experiment

A. Rate constants

Fig. 4 shows a comparison of 6D quantum, RBA and QCT rate constants with those measured in experiment[12] for the $OH + H_2 \rightarrow H_2O + H$ reaction. It can be seen that the agreement between all three methods is good over the 1000 K temperature range considered. This is to be expected as the cumulative probabilities obtained with the three methods agree well. It should be noted that the 6D quantum rate constants were obtained from the cumulative probabilities by the J-shifting approximation[22] and are, therefore, not exact. However, several studies have demonstrated the reliability of the J-shifting approximation for this reaction.[33,34] The fact that at near room temperatures the QCT rate constants are above quantum ones is the reflection of the corresponding trend in QCT cumulative probabilities which was explained in the previous section.

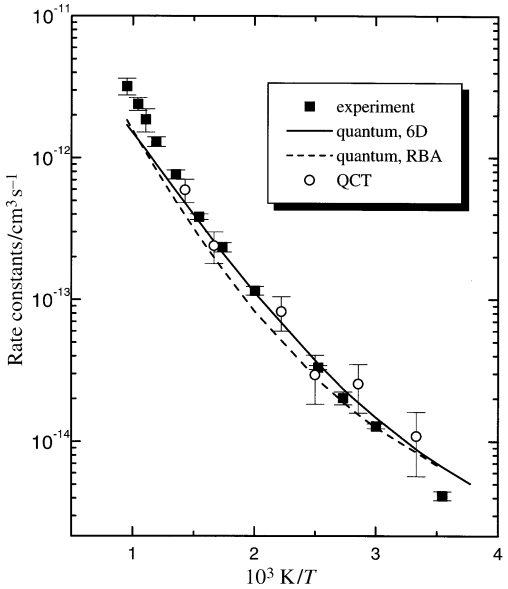

Fig. 4 Arrhenius plot of the calculated and experimental[12] rate constants for the $H_2 + OH \rightarrow H_2O + H$ reaction.

The agreement between the calculated and experimental rate constants is quite good, especially between 330–900 K. In this region the 6D quantum, RBA and QCT rate constants agree with the experimental data within 12, 28 and 27%, respectively. This agreement is superior to that obtained with the SE potential which gave rate constants at least a factor of two above experiment.[5] To calculate the 6D quantum rate constants at temperatures above 1000 K, we have to calculate the reaction probabilities at higher collision energies than reported here. Below 300 K, the rate constants of Fig. 4 are seen to be above experiment, suggesting either that the potential surface allows for too much tunnelling or the vibrationally adiabatic barrier is a little too low. These results emphasise that the OC potential is an improvement on the SE potential but is still not perfect.

B. Differential cross sections

The 6D quantum S matrix elements have so far been calculated for $J = 0$ and thus differential cross sections cannot be extracted from them. RBA calculations, however, can be done for $J > 0$ so that differential cross sections are readily computed.

Fig. 5 compares RBA differential cross sections for the

$$OH + D_2 \rightarrow HOD + D$$

reaction with those measured experimentally.[20] Note that the calculations are for OH in the ground rotational state while the experiments refer to an initial thermal distribution of states. The RBA differential cross sections are obtained in the

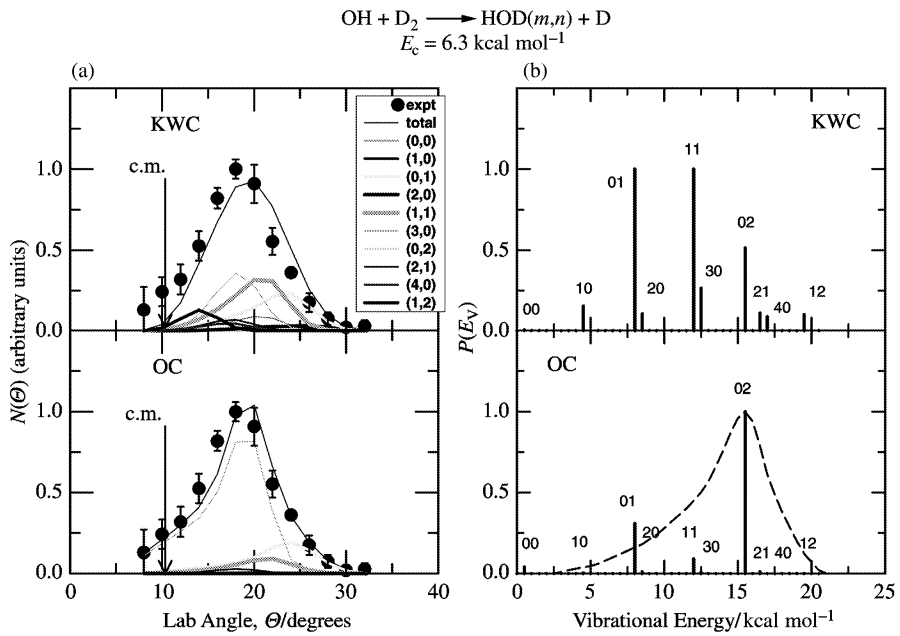

Fig. 5 (a) Comparison of the experimental differential cross sections, in the laboratory frame, for the $OH + D_2 \rightarrow HOD + D$ reaction with RBA calculations. Results obtained using the KWC potential[20] and the OC potential used in the present work[21] are compared. Both total and vibrationally selected differential cross sections are shown. Here (m,n) refers to HOD excited in the bend and local OD stretching modes, respectively. (b) Comparison of experimental (– – –) and calculated (stick diagrams) product vibrational energy distributions with those obtained in RBA calculations using the KWC and OC surfaces. The vibrational states of HOD are labeled by mn.

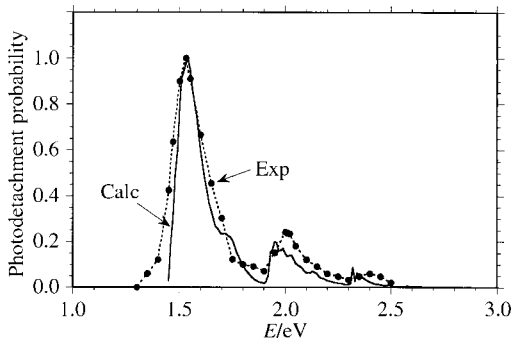

Fig. 6 Calculated spectrum for the photodetachment of H_3O^- to form $H_2O + H$ (——). Also shown in the experimental spectrum (----).[17] The apex of the calculated largest peak has been set to the experimental value.

centre of mass frame and have been converted into the laboratory frame for direct comparison with experiment.[20,35] It can be seen that the agreement is good, and is superior to that obtained with the SE potential and a previous four-dimensional potential (KWC) of Kliesch *et al.*[20]

Fig. 5 also compares RBA and experimental results for the probability distribution of product vibrational energy. Once again the agreement is good and superior to that obtained with the two previous potentials. The HOD state with two quanta in the O–D stretching mode has the highest reaction probability and dominates the translational energy distribution. This, in turn, reflects the significant stretching of the O–H bond formed in the transition state of the reaction.

C. Photodetachment

The measured photodetachment spectra for

$$H_3O^- \rightarrow OH + H_2 + e^- \quad \text{or} \quad H + H_2O + e^-$$

are a very sensitive test of a potential energy surface.[17] Reduced dimensionality calculations on the SE potential showed that this surface gives very poor comparisons with experiment for the photodetachment spectra.[36] RBA calculations using a reduced dimensionality potential obtained from a spline-fit to 3D *ab initio* data give a better comparison.[29] Fig. 6 gives comparison of the experimental[17] photodetachment spectrum for the dominant channel $H_3O^- \rightarrow H_2O + H + e^-$ with that obtained with the RBA using the OC potential. The same H_3O^- potential calculated previously was used in these simulations to calculate the H_3O^- vibrational states.[29] The agreement between the RBA and experimental photodetachment spectra is seen to be very good, including the width of the main peak and the secondary peak corresponding to excitation of the H_2O stretching state. This indicates that the OC potential should be reasonable in the exit channel ($H + H_2O$) of the $OH + H_2 \rightarrow H_2O + H$ reaction away from the transition state.

Classical trajectory calculations have also been done by Lendvay and Schatz on the competition between vibrational energy transfer and reaction in the $H + H_2O$ reaction with H_2O vibrationally excited initially.[37] Comparison with measured rate constants[16] also suggests that the OC potential gives a reasonable description of the $H + H_2O$ channel.

5. Conclusions

One aim of this paper has been to use 6D quantum scattering calculations to test the accuracy of RBA and QCT computations of reaction probabilities for the $OH + H_2 \rightarrow H_2O + H$ reaction using a new OC potential energy surface. Overall, the reaction probabilities compare very well, giving strong evidence that the RBA and QCT methods should be reliable for a four-atom reaction such as this.

In addition, rate constants for the $OH + H_2$ reaction, differential cross sections for $OH + D_2 \rightarrow HOD + D$, and photodetachment spectra for H_3O^- have been calculated and compared with experiment. Overall the agreement between the calculations and experiment for these three very different properties is good, suggesting that the OC potential is certainly reasonable for this reaction and an improvement on previously developed potentials.

Acknowledgements

This work was supported by the Engineering and Physical Sciences Research Council, the National Environmental Research Council, the TMR Programme of the European Union, the British Council and Fundación Antorchas. We are grateful to G. Ochoa for help in using the potential energy surface for the $OH + H_2$ reaction and to P. Casavecchia for processing the differential cross sections to compare with experimental results.

References

1 J. Z. H. Zhang, *Theory and Application of Quantum Molecular Dynamics*, World Scientific, Singapore, 1998.
2 (*a*) D. C. Clary, *J. Chem. Phys.*, 1991, **95**, 7298; (*b*) D. C. Clary, *Chem. Phys. Lett.*, 1992, **192**, 34.
3 J. M. Bowman and D. Wang, *J. Chem. Phys.*, 1992, **96**, 7852.
4 H. Szichman and M. Baer, *J. Chem. Phys.*, 1994, **101**, 2081.
5 U. Manthe, T. Seideman and W. H. Miller, *J. Chem. Phys.*, 1993, **99**, 10078.
6 D. H. Zhang and J. Z. H. Zhang, *J. Chem. Phys.*, 1993, **99**, 5615.
7 S. K. Pogrebnya, J. Echave and D. C. Clary, *J. Chem. Phys.*, 1997, **107**, 8975.
8 D. H. Zhang and J. C. Light, *J. Chem. Phys.*, 1996, **104**, 6184; *J. Chem. Soc., Faraday Trans.*, 1997, **93**, 691.
9 W. Zhu, J. Dai, J. Z. H. Zhang and D. H. Zhang, *J. Chem. Phys.*, 1996, **105**, 4881.
10 J. R. Creighton, *J. Phys. Chem.*, 1997, **81**, 2520.
11 *Rate Coefficients in Astrochemistry*, ed. T. J. Millar and D. A. Williams, Kluwer, Dordrecht, 1988.
12 A. R. Ravishankara, J. M. Nicovich, R. L. Thompson and F. P. Tully, *J. Phys. Chem.*, 1981, **85**, 2498.
13 M. Alagia, N. Balucani, P. Casavecchia, D. Stranges and G. G. Volpi, *J. Chem. Phys.*, 1993, **98**, 2459.
14 M. J. Bronikowski, W. R. Simpson and R. N. Zare, *J. Chem. Phys.*, 1993, **97**, 2194.
15 A. Sinha, M. C. Hsiao and F. F. Crim, *J. Chem. Phys.*, 1990, **92**, 6333.
16 P. Barnes, P. Sharkey, I. R. Sims and I. W. M. Smith, *Faraday Discuss.*, 1999, **113**, 167.
17 E. de Beer, E. H. Kim, D. M. Neumark, R. F. Gunion and W. C. Lineberger, *J. Phys. Chem.*, 1995, **99**, 13627.
18 G. C. Schatz and H. Elgersma, *Chem. Phys. Lett.*, 1980, **73**, 21.
19 G. C. Schatz, M. C. Colton and J. L. Grant, *J. Phys. Chem.*, 1984, **88**, 2971.
20 M. Alagia, N. Balucani, P. Casavecchia, D. Stranges, G. G. Volpi, D. C. Clary, A. Kliesch and H.-J. Werner, *Chem. Phys.*, 1996, **207**, 389.
21 G. Ochoa de Aspuru and D. C. Clary, *J. Phys. Chem. A*, 1998, **102**, 9631.
22 J. M. Bowman, *J. Phys. Chem.*, 1991, **95**, 4960.
23 G. Herzberg, *Infrared and Raman Spectra*, Van Nostrand, New York, 1945.
24 G. C. Schatz, *Chem. Phys. Lett.*, 1988, **150**, 92; G. C. Schatz, *Chem. Phys. Lett.*, 1988, **151**, 409; G. C. Schatz, *J. Chem. Phys.*, 1989, **90**, 3582; G. C. Schatz, *Chem. Phys. Lett.*, 1989, **90**, 4847.
25 A. Kuppermann and P. G. Hipes, *J. Chem. Phys.*, 1986, **84**, 5962; S. A. Cuccaro, P. G. Hipes and A. Kuppermann, 1989, **154**, 155; S. A. Cuccaro, P. G. Hipes and A. Kuppermann, *Chem. Phys. Lett.*, 1989, **157**, 440.
26 G. A. Parker and R. T Pack, *J. Chem. Phys.*, 1993, **98**, 6883.
27 (*a*) J. C. Light and R. B. Walker, *J. Chem. Phys.*, 1976, **65**, 4272; (*b*) E. B. Stechel, R. B. Walker and J. C. Light, *J. Chem. Phys.*, 1978, **69**, 3518.
28 D. C. Clary, *J. Phys. Chem.*, 1994, **98**, 10678.

29 D. C. Clary, J. K. Gregory, M. J. T. Jordan and E. Kauppi, *J. Chem. Soc., Faraday Trans.*, 1997, **93**, 747.
30 J. Palma, J. Echave and D. C. Clary *J. Chem. Soc., Faraday Trans.*, 1997, **93**, 841; note that in the equation for the degeneracy factor, *g*, max should be min.
31 R. N. Porter, L. M. Raff and W. H. Miller, *J. Chem. Phys.*, 1975, **63**, 2214.
32 L. M. Raff and D. L. Thompson, in *The Theory of Chemical Reaction Dynamics*, ed. M. Baer, CRC Press, Boca Raton, FL, 1985, vol. I, p. 1.
33 D. H. Zhang and J. Z. H. Zhang, *J. Chem. Phys.*, 1999, **110**, 7622.
34 D. H. Zhang and S. Y. Lee, *J. Chem. Phys.*, 1998, **109**, 8620.
35 P. Casavecchia, personal communication.
36 W. H. Thompson and W. H. Miller, *J. Chem. Phys.*, 1994, **101**, 8620.
37 G. C. Schatz, G. Wu, G. Lendvay, D. Fang and L. B. Harding, *Faraday Discuss.*, 1999, **113**, 151.

Paper a908080e